JOURNAL OF CATALYSIS 127, 307–331 (1991)

Dynamic CO Oxidation over Pt/Al_2O_3

BERNARD N. RACINE, MARK J. SALLY, BRUCE WADE, AND RICHARD K. HERZ[1]

Chemical Engineering Group, Mail Code 0310, Department of Applied Mechanics and Engineering Sciences, University of California at San Diego, La Jolla, California 92093-0310

Received June 29, 1989; revised August 14, 1990

Dynamic studies of CO oxidation have shown complex behavior such as rate enhancement and CO_2 peak formation during forced-periodic operation. The transient chemical processes which account for this complex behavior during dynamic operation have not been fully identified, indicating the need for further study. In this work, two Pt/Al_2O_3 catalysts, one prepared from a chloride-containing precursor (chloroplatinic acid) and one prepared from a chloride-free precursor (tetraammineplatinum nitrate), were examined in terms of their steady-state reaction behavior and dynamic responses to periodic changes of CO pressure in O_2. During reaction experiments, temperatures ranged from 90 to 190°C, CO pressures ranged from 0 to 0.2 Torr at a constant O_2 pressure of 0.33 Torr, and cycling periods ranged from 5 to 24 s. In addition, adsorption calorimetry and temperature programmed desorption (TPD) experiments were performed to characterize CO adsorption over the catalysts. The results of the steady-state and dynamic reaction experiments correlated with each other and with the adsorption and TPD results and indicated that the sample prepared from tetraammineplatinum nitrate had stronger CO–Pt interactions than the sample prepared from chloroplatinic acid. The two catalysts had similar Pt dispersions, and this comparison shows that measurement of metal dispersion is not sufficient to characterize a supported metal catalyst for CO oxidation. Addition of HCl to the chloride-free catalyst did not have a significant effect on CO adsorption as indicated by TPD. The complex dynamic responses measured over both catalysts demonstrate that transient processes on the catalyst surfaces produced CO_2 at higher rates than would be predicted by instantaneous response to steady-state conditions during dynamic operation.

INTRODUCTION

At a cursory level, the CO oxidation reaction over noble metal catalysts appears to be simple: O_2 adsorbs and dissociates, CO adsorbs, adsorbed CO reacts with adsorbed O atoms, and the CO_2 formed desorbs immediately. The apparent simplicity of the basic mechanism is misleading, however, since the reaction often exhibits very complex behavior: multiple steady states in reaction rate at intermediate CO pressures (*1–5*); self-sustained oscillations in reaction rate under constant feed conditions (*5–12*); and complex behavior during forced dynamic operation (*13–17*). Obviously, information in addition to the elementary steps listed above is required in order to explain the observed behavior.

For example, the list of elementary steps does not specify the detailed ways in which the steps can occur. CO bonds to noble metal surfaces in two configurations, bridged and linear, and has different properties in each of these configurations (*18, 19*). Adsorption sticking coefficients, heats of adsorption, and other kinetic parameters are known to change with surface coverage (*19–21*). A key nonlinear aspect that contributes much of the kinetic complexity is that CO and O_2 have different site-area requirements for adsorption (*22–25*). Adsorbed CO molecules and O atoms can be present on a surface in mixed phases of varying structure and composition (*26, 27*) or segregated in

[1] Author to whom correspondence should be addressed.

0021-9517/91 $3.00

surface "patches" or "islands" (*7, 20, 28–35*) rather than simply being randomly distributed over the surface. A recent analysis by Harold and Garske (*23, 24*) has indicated that one or more of the following additional steps may be necessary to explain steady-state reaction kinetics over wide ranges in conditions: reaction of adsorbed CO with adsorbed molecular O_2, reaction of gas-phase CO with adsorbed O and O_2, and reaction of gas-phase O_2 with adsorbed CO.

Additional complications arise because metal catalyst surfaces usually contain more than one local geometric arrangement of metal atoms, with the different arrangements having different interactions with the reactants (*36–39*). This sensitivity to metal surface structure is especially important for polycrystalline samples and supported metal samples in which wide distributions of metal surface structures are present (*40–43*). Interactions between adsorbed species and metal surfaces can change the structure and composition of the metal surface during reaction (*44, 45*). Reconstruction of surface planes of metal single crystals has been shown to participate in self-sustained oscillations during CO oxidation over Pt by Ertl and co-workers (*11, 12, 46*). Sales, *et al.* (*5*) and Jaeger *et al.* (*47*) have proposed that self-sustained oscillations over the Pt-group metals can arise from transient oxidation and reduction of the metal surface during CO oxidation. Oscillations over Pd(110) resulting from periodic formation and depletion of subsurface oxygen was recently proposed by Ladas *et al.* (*48*). Oxidation of supported Pt has also been observed indirectly (*49, 50*).

Mass and heat transfer resistances coupled with nonlinear surface processes over porous catalysts and nonporous catalysts at high pressure can lead to complex behavior under steady-state (*2, 22, 51*) and dynamic conditions (*52, 53*).

Although much has been discovered about this fascinating reaction system, a comprehensive model has not been developed to explain all of the complex reaction behavior. Questions concerning the clustering of adsorbates on Pt-group metals, the differences between supported crystallites and single crystal surfaces, and the presence of adsorbate-induced surface phase reconstructions on different crystal planes of supported crystallites still exist. The surface processes which lead to self-sustained oscillations over both Pt-group single crystals and supported Pt-group metal catalysts need to be reconciled, and the question of how to model kinetics over the UHV-to-atmospheric pressure range remains. Harold and Garske (*23, 24*) stressed that a comprehensive model will have to fit steady-state kinetics, including rate-multiplicity behavior, over a wide range of conditions. In addition to fitting steady-state behavior over a wide range of conditions, the model must describe self-sustained oscillations. Finally, additional tests of kinetic models should be obtained via forced dynamic response or transient response experiments.

Dynamic Response Methods

In the work reported here, we used forced dynamic response experiments to study CO oxidation over supported Pt. Bennett (*54*) and Kobayashi and Kobayashi (*55*) reviewed the benefits of dynamic response methods in the elucidation of reaction mechanisms. One use of dynamic techniques is determination of the quantities of adsorbed species that are present on a catalyst surface during reaction. The basic principles behind this use can be illustrated by considering the simple example of CO in inert gas flowing over a catalyst without reaction. Under steady-state conditions, the concentration of CO at the inlet of the reactor is equal to the concentration in the effluent, and the amount of CO adsorbed on the surface of the catalyst is unknown unless gravimetric or spectroscopic techniques are available. However, the amount of CO reversibly adsorbed on the catalyst surface can be obtained by stopping the flow of CO to the reactor and recording the CO concentration leaving the reactor during the transition to

the new steady state. During the transition, the CO that was in the void space of the reactor and adsorbed on the catalyst will elute, leading to transient mass balance discrepancies since no CO is entering. The total quantity of CO present in the reactor before the inlet CO was stopped can be determined by integrating the transient mass balance discrepancies. The amount of gaseous CO present in the void space of the reactor can be determined from a transient experiment (done separately or simultaneously) with a nonadsorbing inert tracer and can be subtracted from the total amount to yield the amount adsorbed.

Another advantage of dynamic response techniques is that the rate constants of forward and reverse steps in a reaction mechanism can be determined for some systems in which only the ratio of the rate constants is obtained in steady-state experiments. In the simple example discussed above, analysis of the detailed shapes of the responses to up and down step changes in inlet concentration can give estimates of adsorption and desorption rate constants in favorable cases with no mass transport effects.

Dynamic response experiments in combination with steady-state experiments can provide more severe tests of alternative reaction mechanisms than provided by steady-state experiments alone. An example of the value of dynamic techniques in discriminating between alternative kinetic models is provided by the work of Yang *et al.* (*56*), who studied N_2O decomposition over nickel oxide. They proposed two alternative reaction mechanisms for the decomposition reaction. The rate determining step in both mechanisms is the reaction of N_2O with the surface to produce gaseous N_2 and adsorbed O. In mechanism I, adsorbed O recombines and desorbs as O_2. In mechanism II, adsorbed O is removed by reaction with N_2O to form gaseous N_2 and O_2. Lyberatos *et al.* (*57*) did calculations comparing steady-state rates and transient responses predicted by the two mechanisms proposed by Yang *et al.* They found that the mechanisms are indistinguishable by comparison of steady-state kinetics. The N_2O and N_2 outlet responses to a step-up in inlet N_2O concentration are also very similar for mechanisms I and II. However, the outlet O_2 concentration response has qualitative differences which can be used to discriminate between the two mechanisms. Cutlip *et al.* (*58*) found mechanism I to be superior to mechanism II by comparing model predictions to transient rate data.

Dynamic response techniques have also been used to obtain information concerning mechanisms of CO oxidation over various catalysts. Kobayashi and Kobayashi (*55*) studied CO oxidation over Cr_2O_3, MnO_2, and Pb_3O_4. Steady-state rates over all three materials were first order in CO. However, transient response experiments indicated significant differences in reaction sequence over the three catalysts. The observation of induction times for CO_2 formation following a step-up in O_2 concentration over CO-saturated surfaces indicates that dissociative adsorption of O_2 over Pd/Al_2O_3 (*16*), Pd/SiO_2 (*59*), Pt/SiO_2 (*50, 59, 60*), and Pt/SnO_2 (*61*) is strongly inhibited by adsorbed CO. In the same studies, the absence of observable induction times for CO_2 formation following a step-up in CO concentration over O-saturated surfaces indicates that adsorption of CO over these materials is not inhibited by adsorbed O.

Dynamic CO Oxidation over Supported Noble Metals

Table 1 summarizes investigations of CO oxidation over supported noble metals in which forced dynamic response experiments were performed. Not included in the table are studies where gases other than CO, O_2, and inert were present, studies where reducible base-metal oxides were present in the catalyst, or studies that reported only time-averaged measurements of gas composition.

Complex behavior was observed in each of the works listed in Table 1. Rate enhancements as high as a factor of 20 above those

TABLE 1

Forced Dynamic Investigations of CO Oxidation over Supported Noble Metal Catalysts

Ref.	Catalyst	Temp.	CO (Torr)	O_2 (Torr)	Experiments
(*13*)	Pt/Al_2O_3	28–60°C	15	23	Periodic switching between CO and O_2.
(*16*)	Pd/Al_2O_3	71–133°C	76	76–114	Periodic switching between CO and O_2. Step-up in each component in constant second component. Step-down of CO in constant O_2.
(*14*)	Pt/Al_2O_3	90–120°C	105–126	63–105	Periodic switching between CO and O_2. Periodic switching of CO in constant O_2. Step-up and down of each component in constant second component.
(*62*)	Pt/Al_2O_3	90°C	0–15	0–7.5	Periodic switching between CO and O_2. Periodic switching of CO and O_2 with phase lag. Periodic switching of CO in constant O_2.
(this work)	Pt/Al_2O_3	90–190°C	0–0.2	0.33	Periodic switching of CO in constant O_2.
(*67*)	Pt/Al_2O_3	100°C	0.2–1.2	0.6–1.2	Step change from CO to CO plus O_2; Switching between two CO and O_2 mixtures.
(*59*)	Pt/SiO_2, Pd/SiO_2	80–200°C	38	38	Step change from only CO to only O_2; Step change from only O_2 to only CO.
(*60*)	Pt/SiO_2	100–160°C	15.2	22.8	Step change from only CO to only O_2; Step change from only O_2 to only CO.
(*50*)	Pt/SiO_2	25–192°C	7.6	22.8	Step change from only CO to only O_2; Step change from only O_2 to only CO. Step-up in one component following exposure to steady-state feed of second component and inert flush.
(*89*)	Rh/Al_2O_3	300°C	2.25–12.6	2.25	Step change from one CO value to second CO value at constant O_2. Switching between two CO and O_2 mixtures.
(*49*)	Pt/Al_2O_3	250°C	9.2	9.2	Step-up in CO following exposure to steady-state feed of O_2 and inert flush.
(*65*)	Pt/Al_2O_3	57–377°C	15	7.5	Pulse of one component following pulse of second component and inert flush.
(*88*)	Rh/Al_2O_3	200–500°C	1.5	3	Pulses of $CO–O_2$ mixture into inert carrier gas.
(*53*)	Pt/Al_2O_3	212°C	0–2.4	15.2	Pulse decrease of CO in $CO–O_2$ mixture.
(*75, 76*)	Pt/SiO_2	168–310°C	0–46	0–91	Temperature programming (2.5°C/min) at constant CO and O_2; concentration programming (~20 Torr/h) of CO and O_2 at constant temperature.

possible during steady-state operation were observed by Cutlip (*13*) over Pt/Al_2O_3 as the result of alternate introduction of CO and O_2 to a recycle reactor. Cutlip proposed that the establishment of high surface coverages of O during O_2-half-periods accounted for the increase in conversion over steady-state operation, where high surface coverages of CO inhibit O_2 adsorption. Gulari and coworkers observed a 10-fold rate enhancement over Pt/Al_2O_3 (*14*) as a result of periodic switching between CO and O_2 and a 40-fold enhancement over Pd/Al_2O_3 (*16*). They suggested that a simple enhancement in surface O concentration during O_2-half-periods could not account for such large rate enhancements (*14*) and proposed the formation of new surface structures under dynamic conditions in the form of mixed domains of highly energetic surface CO and O (*16, 17*). Graham and Lynch (*62*) found that varying the phase angle between cycled inputs of CO and O_2 can result in rates 50% greater than those achieved during alternate switching of CO and O_2 or during cycling of CO in constant O_2.

The segregation of adsorbed CO and O into surface patches and islands of adsorbed CO and O has been proposed to explain the results of steady-state and forced-dynamic experiments. Under nonreaction conditions over Pt and Pd, the infrared absorption peak of linearly bonded CO shifts to higher frequencies with increasing CO coverage. Cant and Donaldson (*63*) and Haaland and Williams (*4*) observed that the infrared peak of linearly bonded CO stayed invariant at the high-coverage frequency as the CO coverage changed during steady-state CO oxidation experiments. Similar behavior was observed over a (111)-oriented Pt ribbon by Shigeishi and King (*64*) during exposure of preadsorbed CO to O_2. These observations were explained by the presence of islands of CO during steady-state reaction, with adsorbed CO at high local coverage in the islands.

During forced-periodic reaction experiments over Pt/Al_2O_3, Barshad *et al.* (*15*) also observed frequency invariance of the linearly bonded CO infrared peak and proposed the existence of CO islands under dynamic reaction conditions. Li *et al.* (*59*) made a similar proposal to explain the results of their transient step-change experiments over Pd/SiO_2 and Pt/SiO_2. Su *et al.* (*65*), without benefit of infrared measurements, proposed reaction at the boundary of O islands to explain the results of alternate injection of CO and O_2 over Pt/Al_2O_3. Mundschau *et al.* (*34*) used photoemission electron microscopy to image patches of high oxygen coverage propagating across a CO-covered Pt(100) surface following abrupt decreases in CO pressure during CO oxidation. Rotermund *et al.* (*35*) made similar observations during self-sustained rate oscillations.

The spectroscopic evidence for adsorbate patches and islands has led various investigators to develop mathematical models of CO oxidation that specify the presence of adsorbate islands. A variety of adsorbate island models were used by Mukesh *et al.* (*66*) to model the transient data of Goodman *et al.* (*67*), with the model simulations being most sensitive to the presence of CO islands. Graham and Lynch (*68*) proposed a CO island model to predict steady-state rate multiplicity data which correctly accounted for CO and O surface coverages in the island and nonisland regions. Monte Carlo simulations for CO oxidation have also predicted the formation of adsorbate islands under both steady-state (*69–71*) and transient conditions (*72–74*).

In some cases, conventional Langmuir–Hinshelwood kinetics which assume random distribution of adsorbed species have been used to simulate dynamic CO oxidation behavior. Goodman *et al.* (*67*) used a random Langmuir–Hinshelwood model to describe CO oxidation transients over Pt/Al_2O_3. Kaul *et al.* (*75, 76*) used a random Langmuir–Hinshelwood model to describe the results of temperature and concentration-programming experiments over Pt/SiO_2. Lynch (*77*) also used a random Lang-

muir–Hinshelwood model to simulate rate enhancements for CO oxidation during periodic operation. Cho (*52*) developed a diffusion/reaction model using Langmuir–Hinshelwood kinetics and simulated the evolution of CO and oxygen surface coverage profiles in a porous catalyst during forced concentration cycling.

Using low-energy electron diffraction and work function measurements during reaction, Ertl and co-workers (*11, 78, 79*) showed that self-sustained rate oscillations during CO oxidation over a Pt(100) single crystal surface are associated with reconstruction of the Pt surface between a corrugated hexagonal surface atom arrangement ("hex" surface) and a (1 × 1) surface. The changes in Pt surface structure are induced by changes in CO coverage and affect the reaction rate through a higher O_2 sticking coefficient on the (1 × 1) surface. Ertl and co-workers (*80–82*) have also observed a (1 × 2)–(1 × 1) reconstruction accompanied by microfacetting on Pt(110) single crystal surfaces that similarly affects CO oxidation rates through a higher O_2 sticking coefficient on the (1 × 1) facetted surface.

Schwartz and Schmidt (*83*) suggested that the Pt(100) hex–(1 × 1) surface phase transition may be operative on polycrystalline wires and foils and on supported Pt particles because Pt surfaces tend to facet to predominantly (100) planes in many reactive gases. Schüth and Wicke (*84*) inferred from infrared measurements of the linear CO band the presence of the Pt(100) hex–(1 × 1) reconstruction during self-sustained oscillations of the CO–NO reaction over supported Pt. They did not find evidence for this reconstruction during oscillations of the CO–O_2 reaction, but suggested that reversible microfacetting of Pt(110) planes may have been a factor. Lynch and co-workers incorporated surface reconstruction into a mathematical model which they used to fit data obtained during forced square-wave cycling of CO and O_2 (*62*) and self-sustained oscillations in CO oxidation rate (*85*) over supported platinum catalysts. Direct experimental verification of the presence of reconstruction of supported metal particles under dynamic CO oxidation conditions remains to be performed. However, there is mounting evidence from electron microscopic studies that supported metal particles can change shape and structure in a facile manner under some conditions (*86, 87*).

Current Work

Although previous forced-dynamic studies have demonstrated the complexity of CO oxidation over supported noble metals, questions still remain about the causes of the observed behavior, including whether adsorbed CO and O patches and islands are important during reaction and whether metal crystallite surface reconstruction is important. Many of the previous studies have focused on time-averaged conversion enhancements resulting from forced-periodic operation and were not specifically designed to provide tests of kinetic models. In most cases (*13, 14, 16, 49, 50, 59, 60, 65*) CO and O_2 were fed alternately to the reactor. In these cases, transient peaks in CO_2 production could simply result from "burn-off" or "titration" of adsorbed CO and O by the gaseous coreactant. In work in which both CO and O_2 were present in the gas phase during some periods of operation (*14, 16, 53, 62, 67, 88, 89*), measurements of rates under the corresponding steady-state CO and O_2 pressures were reported in only a few cases (*62, 89*). Such measurements are valuable because they allow the steady-state kinetics and dynamic responses to be compared, revealing important information about transient reaction processes.

In this paper, we examine results of steady-state and forced-dynamic CO oxidation experiments over Pt/Al_2O_3. Both CO and O_2 were present in the gas phase during one portion of each cycling period. Our goals for this work were twofold: first, to compare the behavior of two Pt/Al_2O_3 samples prepared with the same average dispersion but from different Pt precursors, and second, to obtain quantitative measure-

ments under both steady-state and forced-dynamic conditions that can be used to test kinetic models in future work.

We studied two Pt/Al_2O_3 samples prepared from chloride-containing and chloride-free Pt precursors frequently used in catalyst preparation, and compared the behavior of the two catalysts. Large differences between the chloride-containing catalyst and the chloride-free catalyst were observed in both the steady-state and dynamic reaction experiments. To further characterize the differences in reaction behavior, adsorption calorimetry and temperature programmed desorption (TPD) experiments were performed. TPD was also performed to determine whether sample characteristics changed with time over the course of the dynamic and steady-state studies. In our experiments, catalyst surfaces were stable over time, as indicated by reproducible day-to-day TPD spectra, both before and after reaction experiments. Another reason for performing adsorption calorimetry and TPD measurements is that CO adsorption and CO surface coverages dramatically affect CO oxidation kinetics. We wanted to determine whether CO adsorption measurements from calorimetry and TPD experiments correlated with reaction results. Good correlation was obtained between the results of the different types of experiments. In addition, dynamic experiments showing the effects of both temperature and cycling time on reaction behavior were performed.

EXPERIMENTAL

Reactor Design

The experimental apparatus was designed to perform adsorption calorimetry, thermal desorption, and reaction studies on a sample without transfer or exposure of the sample to air between experiments and with minimum elapsed-time between experiments.

The sample chamber used for the experiments is shown in Fig. 1. It consisted of a stainless steel UHV cube, 7 cm on a side, with two glass viewports on opposite sides. All components of the system were either standard UHV components or made from UHV-compatible materials. A thin, pressed wafer of catalyst was suspended in the center of the chamber by the leads of a fine thermocouple pressed into the center of the sample. The thermocouple leads were connected to feedthroughs on the top flange of the sample chamber. Sample heating was accomplished with two tungsten–halogen lamps (Oriel, Inc. Model 6334) in elliptical reflectors (Melles Griot, Inc. Model 02 REM 001) focused on the sample through the glass viewports. A gate valve on the bottom flange of the sample chamber connected the sample chamber to the lower UHV chamber, which contained a quadrupole mass spectrometer and a 110-liter/s turbomolecular pump.

The flange on the right side of the sample chamber was linked to a right angle valve and a 50-liter/s turbomolecular pump. A 4-mm-i.d. stainless steel tube exiting the bottom right corner of the sample chamber provided a connection to the lower chamber through a shut-off valve and an orifice gasket. Gases were fed to the sample chamber through a six-way cross connected to the left side of the chamber. Two of the flanges on the cross were attached to piezoelectric valves (Perkin–Elmer Model PV-10) to allow computer control of the O_2 and CO flows. A third flange on the six-way cross was attached to a manual leak valve to regulate H_2 pressure in the chamber during daily pretreatment procedures. The CO and O_2 cylinder specifications were 99.99% purity and the H_2 cylinder specification was 99.9995% purity. A fourth flange on the six-way cross was attached to a 0–1 Torr capacitance manometer.

An IBM PC with a Data Translation, Incorporated interface board was used to control the sample temperature. A control signal from the computer powered the heating lamps through a programmable 2 kW dc power supply. A second IBM PC interfaced to the system controlled the piezoelectric valves and the mass spectrometer and re-

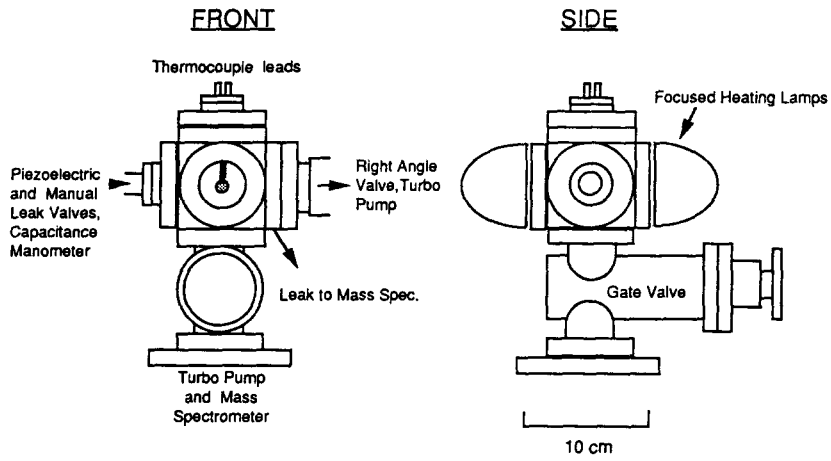

FIG. 1. Sample chamber. All components are UHV compatible.

corded the sample temperature and mass peak intensities.

The characteristic time for diffusion of CO and O_2 in the chamber under reaction conditions is L^2/D. For a length, L, of 3.5 cm, one-half the chamber width, and a diffusivity, D, of 340 cm^2/s at 0.5 Torr, the diffusion time is 0.04 s. The sample chamber was assumed to be a well-mixed CSTR, based on the small diffusion time relative to the mean gas residence time of 1.0 s used in all reaction experiments.

Under some conditions with the positive–negative-order kinetics characteristic of CO oxidation, it is possible to have multiple steady states of conversion in CSTRs (*1*). Multiple steady states in CSTRs are possible even when the intrinsic or internal-diffusion-limited kinetics by themselves do not exhibit multiplicities. Such multiple steady states due to the interaction between positive–negative-order catalyst kinetics and the "mass balance operating line" of a CSTR mainly occur at relatively low catalyst-based space velocities (*90*). The catalyst-based space velocity in our system was very high, 6×10^4 cm^3-gas/cm^3-catalyst · s, our conversion levels were always low, <3%, and we did not observe, nor attempt to obtain, multiple steady states in our studies.

Gradients in reactant gas concentration over the external surface of the catalyst wafers were estimated by modeling the system as a catalyst pellet in a large stagnant gas reservoir with no convective contribution to reactant transport to the surface (*91*). An overall first-order rate constant was determined from the steady-state rate data measured over the chloride sample. Reactant concentrations at the external surface of the catalyst wafers were estimated to be 99% of the average bulk gas concentrations, indicating that external mass transfer resistance was negligible at the low gas pressures and high reactant diffusivities present in the reactor.

As in any reactor design, tradeoffs had to be made during the design in order to accomplish as many of the desired goals as possible. The one design goal not achieved was the elimination of internal concentration gradients. Using a pseudo-first-order rate constant determined from the steady-state reaction experiments reported below, a characteristic sample half-thickness of 0.019 cm, and an effective diffusivity of 0.125 cm^2/s, the value of the Thiele modulus for a typical sample under steady-state reaction conditions was estimated to be between 2 and 3. The effective diffusivity used in the calculation was based on mercury porosimetry measurements on approximately 1 g of pressed wafers. The porosimetry mea-

surements yielded a total pore volume for macropores of 0.20 cm^3/g, a total pore volume for micropores of 0.24 cm^3/g, an average macropore diameter of ~500 nm, and an average micropore diameter of ~8 nm. Although internal diffusional limitations were present under some conditions, these limitations do not alter the qualitative comparisons presented here. Specific effects of diffusional limitations in this study are discussed in the Results and Discussion section of the paper.

The sample was heated uniformly by aligning the tungsten–halogen lamps such that the sample was located slightly in front of the focal point of each of the reflectors. Prior to experimentation, a white screen was placed directly in front of the sample, and the light projected onto the screen uniformly illuminated an area somewhat greater than that of the sample. The maximum temperature gradient possible across the thickness of a sample was estimated from $\Delta T = \Delta H D_e C_s / \lambda_e$, where ΔH is the heat of reaction (kcal/mol), D_e is the effective diffusivity (cm^2/s), C_s is the concentration of CO gas at the external surface of the sample (mol/cm^3), and λ_e is the effective thermal conductivity of the sample (kcal/cm · s · °K). The maximum temperature gradient possible across the sample during CO oxidation was estimated to be 0.6°C, a temperature difference found to be negligible during measurements of steady-state reaction rates. The characteristic time for heat to propagate through the sample was estimated using $t = L^2 \rho C_p / \lambda_e$, where L is the half-thickness of the sample (cm), ρ is the density of the sample (g/cm^3), and C_p is the heat capacity of the sample (kcal/g · °K). The thermal time was calculated to be approximately 0.4 s, which is small compared to the time periods of the dynamic experiments.

Catalyst Preparation

The incipient wetness impregnation technique was used to prepare both samples in this study, a 2 wt% Pt/Al_2O_3 catalyst from H_2PtCl_6 ("chloride" sample) and a 1 wt% Pt/Al_2O_3 catalyst from $(NH_3)_4Pt(NO_3)_2$ ("nitrate" sample). The support material for both catalysts was Alfa Products No. 89372 gamma-alumina pellets, with a surface area of 100 m^2/g. The alumina pellets were ground and sieved and the 200/150 mesh fraction used for impregnation.

For the chloride sample, chloroplatinic acid ($H_2PtCl_6 \cdot 6H_2O$, 39.47% Pt by weight) from AESAR was used for the impregnation. For the nitrate sample, tetraamineplatinum nitrate ($(NH_3)_4Pt(NO_3)_2$), 48.95% Pt by weight) from AESAR was used. Each powdered metal compound was dissolved in deionized water and then added to the alumina to incipient wetness. The samples were then dried in air at 100°C overnight. The pretreatment procedure for the dried catalyst was: (a) heat at 10°C/min to 400°C in 5% O_2 in flowing He at 760 Torr (1 Torr = 133.3 N/m^2), hold for 4 h, ramp down to 25°C at 10°C/min, then flush with pure Ar; (b) switch to 5% H_2 in Ar, ramp at 10°C/min to 300°C, hold for 2 h; (c) switch to pure Ar for 15 min flushing, ramp down at 10°C/min to 25°C; and (d) switch to 0.01% O_2 in Ar for surface passivation for 20 min.

To form a sample wafer, a desired amount of pretreated sample (10–15 mg) was weighed for loading into a steel die. The die was machined so a chromel-alumel thermocouple, 0.05 mm in diameter, could be pressed into the center of the wafer. The sample was pressed in the die at 3 metric tons for 2 min, and the resulting wafer was 5 mm in diameter and approximately 0.38 mm in thickness.

Experimental Procedure

At the start of each day of experimentation, samples were (a) pretreated in vacuum (~10^{-7} Torr) at 550°C for 1 h, then cooled to room temperature; (b) ramped at 60°C/min in 1 Torr O_2 to 375°C and held for 1 h, then cooled; (c) ramped at 60°C/min in 1 Torr H_2 to 300°C and held for 1 h, then cooled; and (d) ramped to 450°C at 60°C/min in vacuum to desorb H_2 and H_2O.

To begin an adsorption calorimetry experiment, both the right angle valve and the

gate valve were closed as the sample cooled from a preceding desorption experiment. When the sample temperature reached a specified temperature (about 30°C), the CO piezoelectric valve was opened briefly by the computer to admit 0.78 Torr of CO into the isolated sample chamber. After recording the sample temperature vs time, the CO gas in the chamber was pumped out and a TPD experiment was performed. The temperature ramp for the TPD runs was 1°C/s. Total pressures in the lower chamber during TPD runs ranged from 6×10^{-8} to 2×10^{-6} Torr.

The sensitivity of the mass spectrometer was determined in the following manner: A sample of Pt/SiO_2 with a known CO uptake (*92*) was placed inside the sample chamber. The sample was saturated with CO at room temperature, and a linear temperature ramp was applied to desorb the CO from the catalyst. The CO signal from the mass spectrometer was recorded as a function of time, and the area under the curve (after subtraction of a desorption spectrum from pure SiO_2) was determined. From this method, the sensitivity (μmol CO/V · s) at constant pumping speed was calculated. The sensitivity was held constant from day-to-day by establishing a constant pressure of 0.5 Torr of CO in the upper chamber and a constant leak through the orifice gasket to the mass spectrometer in the lower chamber. The high voltage on the mass spectrometer's electron multiplier was then adjusted to give an output signal voltage that was held constant from day-to-day.

Using the known sensitivity of the mass spectrometer, voltage vs time plots during CO TPD experiments with unknown samples could then be integrated to obtain the amount of CO adsorbed on each catalyst. By comparing the amount of CO adsorbed to the amount of Pt in each sample, and assuming a one-to-one ratio of CO molecules adsorbed per Pt atom exposed, the percentage of Pt exposed ("dispersion") could then be calculated. Using this technique, the chloride sample was found to have an average Pt dispersion of 85 ± 6%, and the nitrate sample was found to have an average Pt dispersion of 84 ± 7%.

For the reaction studies, the right angle valve connected to the top turbo pump was adjusted to establish the same constant volumetric flow rate for each experiment, and the gate valve to the lower chamber was closed. The orifice gasket provided a constant leak to the mass spectrometer during reaction experiments. Total pressures in the upper chamber for the reaction experiments ranged from 0.33 to 0.53 Torr. The total volumetric flow rate used for the steady-state and dynamic reaction experiments was 0.87 liter/s. This flow rate was calculated using an estimate of the chamber volume (0.87 liter) and a measurement of exponential response time (1.0 s) observed as the inlet flow of gas was abruptly turned off.

RESULTS AND DISCUSSION

Steady-State Reaction Experiments

For the steady-state reaction experiments, conditions of constant O_2 pressure (330 mTorr) and constant catalyst temperature (145°C) were established for experiments on both the chloride and nitrate samples. Reaction rates were then determined at various steady-state CO pressures over the range of CO pressures used in the dynamic reaction experiments described below. Full surveys to determine limits of the positive-order, negative-order, and multiple steady-state regimes were not performed. Neither hysteresis nor oscillations were found for either sample over the range of conditions (0–200 mTorr CO) studied.

Figure 2 shows CO_2 pressure as a function of CO pressure for both the chloride and nitrate samples under steady-state conditions. The reaction rate is proportional to the product of the CO_2 pressure and the volumetric flow rate (0.87 liter/s). A direct first-order relationship between CO_2 production and CO pressure was observed over the chloride sample (Fig. 2a). Over the nitrate sample (Fig. 2b), the reaction was found to be zero order in CO pressure, ex-

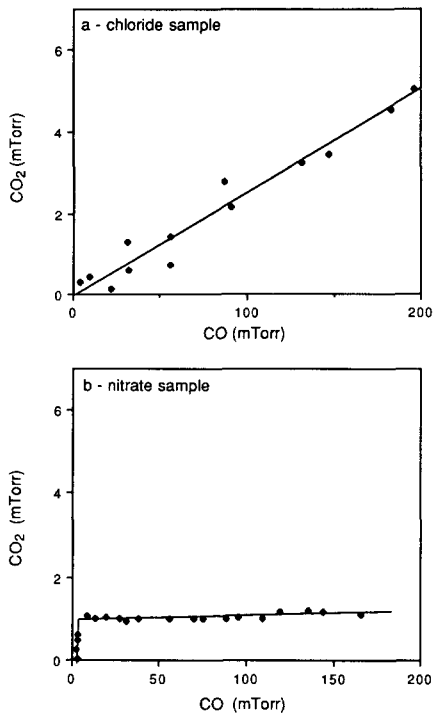

FIG. 2. Steady-state CO_2 pressure vs CO pressure for (a) the chloride sample and (b) the nitrate sample at 145°C and 330 mTorr O_2. The total volumetric flow rate through the sample chamber was 0.87 liter/s.

cept for a positive-order region between 0 and 5 mTorr of CO.

Steady-state CO oxidation over supported noble metals has been studied extensively and the general features are understood reasonably well (*22*). At fixed O_2 pressure and temperature and relatively low CO pressures, reaction rates are approximately first order in CO pressure, O coverages are high, and CO coverages are low. At relatively high CO pressures, reaction rates become negative order in CO pressure, O coverages are low, and CO coverages are high.

First-order kinetics persist to higher CO pressure as O_2 pressure increases, as temperature increases, and as the adsorption bond energy of CO decreases. The result that the chloride sample exhibited first-order kinetics under the same conditions that the nitrate sample exhibited zero-order kinetics indicates that the adsorption bond energy of CO over the chloride sample was lower than over the nitrate sample. In other words, the comparison in Fig. 2 indicates that the Pt in the nitrate sample adsorbed CO more strongly, on average, than the Pt in the chloride sample.

The zero-order kinetics observed with the nitrate sample are unusual. Zero-order behavior in CO oxidation kinetics is usually observed over a relatively narrow range of CO pressure in the transition region between first-order and negative-order kinetics. Internal diffusion resistance, however, tends to drive negative-order intrinsic kinetics toward first-order behavior. In fact, steady-state behavior similar to that observed over the nitrate sample might possibly result from the coupling of internal diffusional resistance with relatively simple CO oxidation kinetics. Wei and Becker (*51*) examined the effect of diffusion on overall reaction rate for CO oxidation in porous catalysts. Overall rates of reaction were calculated using an empirical intrinsic rate expression: $R = k_r P_{co}/(1 + K_a P_{co})^2$, where k_r is a rate constant, K_a is the CO adsorption equilibrium constant, and P_{co} is the CO pressure. Figure 3 shows overall rates of reaction obtained using effectiveness factors calculated by Wei and Becker for two cases. In the two cases, the functional form of the intrinsic rate expression and the internal diffusion resistance (Thiele modulus ϕ) were the same, however, the rate parameters k_r and K_a differ.

Curve (a) in Fig. 3 shows first-order behavior similar to that of the chloride sample. Curve (b) shows a weak variation in overall rate with CO pressure, similar to the behavior exhibited by the nitrate sample. The differences between curve (b) and the behavior of the nitrate sample may be due to the presence of more complex intrinsic kinetics in the nitrate sample. For example, the presence of a distribution of sites in the nitrate sample with different CO adsorption energies, as indicated by the TPD results pre-

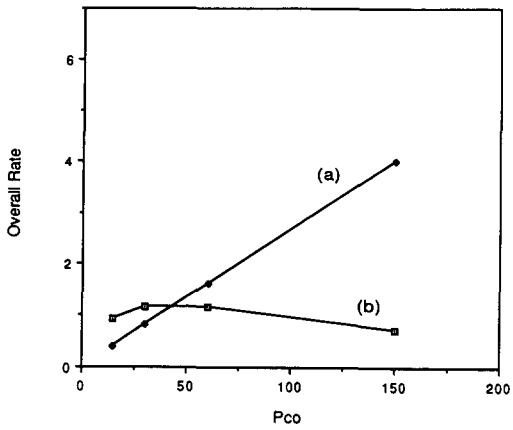

FIG. 3. Calculated overall rate vs CO pressure (in arbitrary units) that would be observed over a porous catalyst using an empirical intrinsic rate expression and effectiveness factors from Wei and Becker (*51*). The intrinsic rate expression, $R = k_r P_{co}/(1 + K_a P_{co})^2$, when coupled with internal diffusion resistance, yields both first-order and approximately zero-order behavior for two cases with the same diffusion resistance (Thiele modulus $\phi = 2$) but different intrinsic rate parameters. For curve (a) $K_a = 0$ and $k_r = 0.0533$; for curve (b) $K_a = 30$ and $k_r = 5.11$.

sented below, could have resulted in a compensating shift between the proportions of sites exhibiting positive-order kinetics and those exhibiting negative-order kinetics as the CO pressure changed. The fact that the CO adsorption equilibrium constant K_a for curve (b), which resembles the behavior of the nitrate sample, is greater than the constant for curve (b), which resembles the behavior of the chloride sample, provides additional support to the preliminary conclusion that the Pt in the nitrate sample adsorbed CO more strongly, on average, than the Pt in the chloride sample.

Dynamic Reaction Experiments

A principal objective of performing dynamic reaction studies is to determine whether transient chemical processes affect catalyst activity. The actual response of a catalyst sample under dynamic conditions in an experiment is referred to here as the "measured response." The "instantaneous response" of the sample is the response that would have been obtained if the catalyst sample were to have been exposed to the same conditions which existed at each instant during the dynamic experiment and the catalyst performance in each instant were that obtained under the corresponding steady-state conditions (*93, 94*). In this study, the "instantaneous response" of a sample in an experiment could be calculated directly from the measured reactant pressures during the experiment and the steady-state data shown in Fig. 2. Differences between the measured and instantaneous responses result from transient chemical processes which occurred during the experiment. "Extra" CO_2 production refers to measured CO_2 production during a dynamic experiment that is greater than the level of CO_2 production predicted by the catalyst's instantaneous response. This instantaneous response method has been used in the past for analyzing the dynamic behavior of automobile catalysts (*93, 94*). Care must be taken so that the catalyst does not show steady-state oscillations, and, if the system exhibits hysteresis, the directionality of transients must be taken into account to correctly analyze the dynamic response.

The principal dynamic reaction studies were performed at the same temperature and O_2 pressure used for the steady-state reaction analysis: 145°C and 330 mTorr of O_2. The CO inlet valve was opened and closed between settings that would give steady state CO pressures of 120 and 0 mTorr. The cycling period was 24 s with a 50% duty fraction. Following 5 cycles prior to the start of data acquisition, the catalyst response was averaged over the subsequent 20 cycles. The plots shown in Figs. 4–8 show the averaged responses of the catalysts over one cycle of the periodic input.

Figure 4 shows the CO input and the measured CO_2 response of the chloride sample. Note that the CO input approximated a square wave with only a slight overshoot in CO pressure, yet the CO_2 response showed two peaks, one approximately 3.5 s follow-

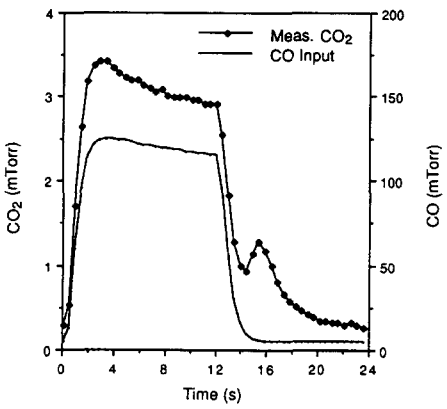

FIG. 4. CO input and CO_2 response of the chloride sample over a 24-s cycle. The CO pressure was periodically cycled between 0 and 120 mTorr with a 50% duty fraction while the O_2 pressure was held constant at 330 mTorr. A single cycle is shown that is the average of 20 successive cycles. The catalyst temperature, T, was 145°C.

ing the onset of CO into the sample chamber, and another peak approximately 3.5 s after CO was switched off. Peaks resembling those observed here were observed by Barshad and Gulari (*14*) during transient cycling of CO at constant O_2 pressures for similar cycling times and duty fractions. However, their peak maxima occurred about 10 s following each change in the CO concentration, probably because their temperatures were lower and CO pressures higher than those used here.

Figure 5 shows the CO_2 response and temperature of the chloride sample as a function of time during a cycle. The temperature changes resulted from changes in heat generation by reaction and changes in cooling by the gas surrounding the sample and were only ± 0.5°C. During the steady-state experiments, changes in temperature of ±0.5°C were deliberately made but negligible changes in reaction rate were observed. Therefore, the samples can be considered nearly isothermal and the peaks shown in Figs. 4–6 were not caused by or significantly affected by fluctuations in catalyst temperature. In particular, the 0.6°C temperature rise that occurred after CO was turned off at 12 s in Fig. 5 was not the cause of the peak in CO_2 production at 15.5 s into the cycle: assuming a conservative 120 kJ/mol activation energy, a 0.6°C temperature rise would cause only a 5% increase in rate; a 40% increase was observed.

Figure 6a shows both the measured and instantaneous CO_2 responses for the chloride sample during the 24-s cycling experiment. The instantaneous response was computed from the first-order steady-state behavior shown in Fig. 2a. The difference between the two curves is the "extra" CO_2 produced as the result of transient chemical processes. Again, note the extra CO_2 production seen for the chloride sample following both the onset of CO into the reactor and flushing of CO from the reactor. The difference between the two curves in the 2–6 s region indicates that the CO_2 peak formed in this region is not due to the slight overshoot in CO pressure seen in Fig. 4. The sharp peak in the measured CO_2 response at 15.5 s into the cycle in Fig. 6a is especially intriguing. The presence of this peak emphasizes the result that transient chemical processes are occurring under dynamic conditions that cannot be predicted from the steady-state behavior.

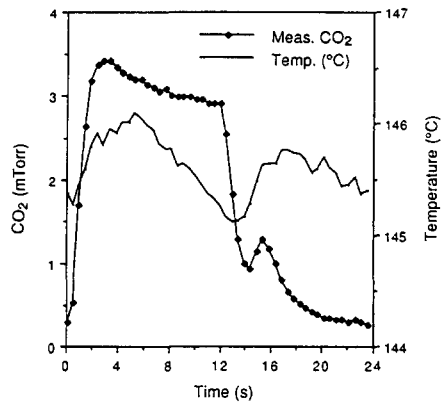

FIG. 5. Catalyst temperature fluctuation and CO_2 response over the chloride sample for the 24-s cycle experiment between 0 and 120 mTorr CO with a 50% duty fraction. O_2 pressure = 330 mTorr.

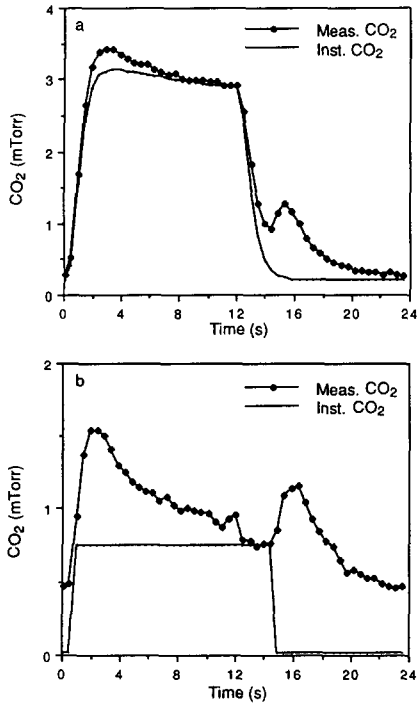

FIG. 6. Measured and instantaneous CO_2 responses over the 24-s cycle between 0 and 120 mTorr CO with a 50% duty fraction for (a) the chloride sample and (b) the nitrate sample. T = 145°C and O_2 pressure = 330 mTorr.

Figure 6b shows the measured and instantaneous CO_2 responses for the nitrate sample under identical conditions as those in Fig. 6a. The instantaneous response was essentially a constant CO_2 level while CO was present in the chamber due to the zero-order steady-state dependence on CO pressure. The peaks in Fig. 6b for the nitrate sample are much broader than those for the chloride sample in Fig. 6a, and extra CO_2 production occurred over the entire period in which CO was present in the sample chamber. Also, note that CO_2 production increased over the nitrate sample immediately as CO was switched off, whereas, over the chloride sample, the second peak occurred only after CO_2 production had begun to decline sharply.

Since the steady-state kinetics observed over the nitrate sample are unusual, an additional dynamic experiment was conducted to check the steady-state results. Figure 7 shows a plot of CO and CO_2 pressures over the nitrate sample during a cycling experiment under the same conditions as Fig. 2, except the CO input was cycled between two nonzero pressures, 40 and 90 mTorr. The results show no significant change in CO_2 signal, confirming the zero-order steady-state behavior shown in Fig. 2b.

Figure 8 shows the differences between the measured and instantaneous responses shown in Fig. 6. Note that, in Fig. 6, the activity level of the nitrate sample is lower than that of the chloride sample, however, in Fig. 8, the extra CO_2 peaks for the nitrate sample are larger. Integration of the extra CO_2 peak following onset of CO over the choride sample yields a magnitude of 0.08 monolayer, where we define for use here that one "monolayer" for a sample is equivalent to the amount of CO that is adsorbed by the sample at saturation coverage as determined by TPD. The first extra CO_2 peak for the nitrate sample has a magnitude of 0.35 monolayer. Integration of the second extra CO_2 peaks following switching-off of CO during each cycle yields a peak that is

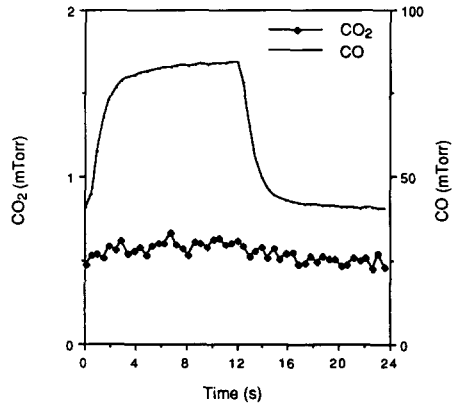

FIG. 7. CO input and CO_2 response for the nitrate sample to a 24-s–50% duty fraction cycle between 40 and 90 mTorr CO. T = 145°C and O_2 pressure = 330 mTorr.

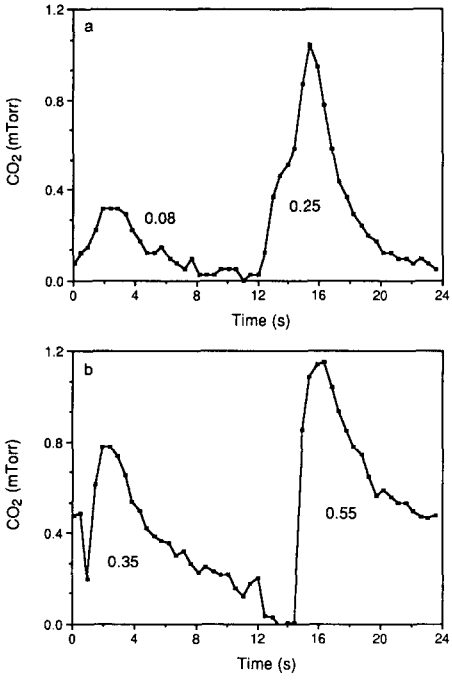

FIG. 8. "Extra" CO production for the 24-s–50% duty fraction cycling experiment at 145°C and 330 m Torr O_2 for (a) the chloride sample and (b) the nitrate sample. The number next to each peak refers to the amount of extra CO_2 produced in the peak in units of "monolayers."

0.25 monolayer for the chloride sample, compared to 0.55 monolayer for the nitrate sample.

Interpretation of Dynamic Experiments

The extra CO_2 peaks observed during dynamic operation may be affected by a number of different phenomena which have been identified in the Introduction and will be discussed below. Regardless of the identity of the individual phenomena that contribute to the detailed shapes of the dynamic responses observed, we expect from previous studies (*13, 14, 16, 50, 59, 60, 65*) that a significant fraction of the extra CO_2 that was observed was due to "burn-off," or "titration" of adsorbed CO and O during transitions to new conditions and new surface coverages. Specifically, we expect that a major fraction of the first extra CO_2 peaks was due to removal of excess adsorbed O by reaction with CO as CO was turned on. A major fraction of the second extra CO_2 peaks is probably due to removal of adsorbed CO by reaction as CO is turned off. Although measurement of transient mass balance discrepancies reveals the presence of such burn-off, titration, or "accumulation-reaction" processes during dynamic experiments (*94*), conversion levels were too low in this work, <3%, to allow accurate transient mass balances to be made. However, under the assumption that burn-off of adsorbed CO was significant as CO was turned off, a comparison of the second extra CO_2 peaks suggests that the nitrate sample had a higher coverage of adsorbed CO on its Pt surface during reaction just before the CO was turned off than did the chloride sample: the second extra CO_2 peak had a magnitude of 0.55 monolayer for the nitrate sample and 0.25 monolayer for the chloride sample. This comparison suggests that the Pt in the nitrate sample adsorbed CO more strongly, on average, than the Pt in the chloride sample. This is the same preliminary conclusion reached above by comparison of the zero-order steady-state kinetics observed over the nitrate sample with the first-order kinetics observed over the chloride sample.

In continuing work, we are performing numerical simulations of the steady-state behavior and dynamic responses reported here. Our first objective is to determine whether or not the results reported here can be explained by conventional "random Langmuir–Hinshelwood kinetics" (*22–24*) which assume coverage-independent rate parameters and random distribution of adsorbed CO and O over a uniform surface of constant activity. Initial simulations indicate that such simple kinetics cannot explain our experimental results. The combination of random Langmuir–Hinshelwood kinetics with a distribution of Pt particle sizes and, therefore, a distribution of surface structure

and activity will also be explored. In further simulations, the possible participation of patches or islands of adsorbed CO and the possible participation of transient Pt surface reconstruction will be explored. These phenomena are discussed later in this section. The various mathematical models to be developed in the simulation work can later be used to design new experimental tests of the various mechanistic possibilities.

The numerical simulations we are performing account for diffusion of gaseous CO and O_2 as well as reaction in the porous samples. Whereas we are certain that diffusional limitations affected the shapes of the dynamic responses observed, we doubt that diffusional limitations were the cause of the extra CO_2 peaks reported here. Diffusional limitations can lead to high CO gas concentrations and high CO coverages near the outer surface of the catalyst, but low CO concentrations and low CO coverages inside the catalyst. Under some conditions, this could result in first-order-overall steady-state kinetics, as observed over the chloride sample, but high fractional burn-off of adsorbed CO during transients. This scenario, however, is not consistent with the observed delay in the appearance of the extra CO_2 peak over the chloride sample after CO gas is flushed from the reactor. Reaction of high outer surface coverages should lead to the appearance of the CO_2 peak immediately following the drop in CO pressure. Also, CO_2 peaks similar to ours have been observed with very different catalyst and reactor geometries by Barshad and Gulari (*14*) and Graham and Lynch (*62*).

In addition to diffusional effects, the possible presence of spurious effects caused by macroscopic nonuniformities in the catalyst wafers used must be considered. Pawlicki and Schmitz (*95*) used infrared thermography to study the H_2 oxidation reaction over Pt/Al_2O_3 and demonstrated that macroscopic nonuniformities in catalyst activity and porosity and, thus, temperature during reaction can occur across a catalyst wafer. If macroscopic nonuniformities were present in our samples, they might have contributed to the extra CO_2 peaks we observed. However, although perfectly uniform samples are never achieved, we believe that the extra CO_2 peaks we observed were not caused by macroscopic nonuniformities. First, we obtained similar steady-state and dynamic results over two different chloride sample wafers pressed from the same starting powder. Second, CO_2 peaks similar to ours have been observed with very different catalyst and reactor geometries by Barshad and Gulari (*14*) and Graham and Lynch (*62*). Also, the catalyst wafers used in (*95*) were 10 times larger (2 cm × 2 cm) than the catalyst wafers used in our study (0.5 cm in diameter), and large pressed catalyst wafers are expected to be more subject than small-diameter wafers to nonuniformities in porosity caused by nonuniform pressures during pressing. The sizes of the hot spots in the large wafer observed in (*95*) were roughly the size of our entire sample. In addition, the spatial variations in temperature observed by Pawlicki and Schmitz for H_2 oxidation over Pt/Al_2O_3 wafers (*95*) and Kaul and Wolf for CO oxidation over Pd/SiO_2 wafers (*96*) were accompanied by steady-state rate multiplicities and self-sustained oscillations; however, rate multiplicities and oscillations were not observed in our experiments. These works were also performed at or near atmospheric pressure in contrast to the low pressures (ca. 0.5 Torr) used here. Tsai *et al.* (*25*) proposed that increased coupling between nonuniformities through the gas phase at low pressure tends to synchronize the nonuniformities, and Lindstrom and Tsotsis (*97*) found that oscillations in CO oxidation rate over a Pt/Al_2O_3 waver were spatially uniform at 1–10 Torr. Nevertheless, (*95*) and (*96*) demonstrate that nonuniformities should be an ever-present concern during studies of porous catalyst and, as we have shown in other work (*98*), during studies of polycrystalline metal catalysts.

One phenomenon we are exploring in our numerical simulations is the possible partici-

pation of patches or islands of adsorbed CO (the experiments performed here, CO cycling in constant O_2, are expected to be less sensitive to the presence of adsorbed O patches and islands). First-order behavior, such as that observed over the chloride sample, is usually thought to exist only under low surface coverages of CO. Traditional random Langmuir–Hinshelwood kinetic models assume independent, identical lattice sites for adsorption, one adsorbed molecule per site, random distribution of adsorbates, and no lateral interactions between adsorbates. Variations of this type of model, such as those proposed by Herz and Marin (*22*) for steady-state reaction data, indicate that in regions of first-order behavior, coverages of less than 0.05 monolayer of adsorbed CO exist on the surface. Coverages between 0.1 and 0.7 monolayer of CO, such as those suggested here for the chloride sample, are predicted by random Langmuir–Hinshelwood models only in unstable steady-state regions between first-order and negative-order behavior. The indication that CO coverages over the chloride sample may be as high as 0.25 monolayer in the presence of first-order kinetics suggested to us that segregation of adsorbed CO and O may be occurring. Adsorbed CO segregated in patches or islands would inhibit dissociative adsorption of O_2 less than randomly distributed adsorbed CO. CO adsorbing in the surface "sea" between islands would react immediately with adsorbed O, contributing to first-order behavior. The contribution of reaction at the perimeter of adsorbed CO patches would change with time during transients as the perimeter length changed with island growth and coalescence or shrinkage and breakup. Our preliminary numerical simulations suggest that the presence of maxima in patch or island perimeter lengths at intermediate CO coverages could potentially cause the appearance of extra CO_2 peaks during both CO-on and CO-off transitions.

The samples studied here had an average Pt dispersion of about 85%. The average Pt particle diameter corresponding to this dispersion is about 1.2 nm. More than one island of adsorbed CO would be difficult to fit on a 1.2 nm particle. A more likely scenario would be, for example, a single reaction front of an advancing adsorbed-O-rich region propagating across a CO-covered particle as gas-phase CO is flushed from the reactor. This scenario is similar to one proposed by Cant and Donaldson to explain frequency invariance of CO infrared peaks during changes in CO oxidation conditions over Pt/SiO_2 (*63*). Recently, the propagation of CO oxidation reaction fronts across large Pt single crystal surfaces has been convincingly demonstrated by Mundschau *et al.* (*34*) and Rotermund *et al.* (*35*) who used spatially resolved photoemission electron microscopy to image propagating reaction fronts.

Another process whose contribution we will explore in future numerical simulations is adsorbate-induced surface reconstruction. A kinetic model describing surface phase transformation was developed originally by Ertl *et al.* (*11*) to explain oscillatory behavior on Pt(100) and was applied by Lynch and co-workers (*62, 85*) to explain oscillations and forced transient behavior on supported metal catalysts. The model, in effect, states that when the surface coverage of CO increases above a critical value, a Pt(100) surface reconstructs from a corrugated hexagonal surface atom arrangement ("hex" surface) to a (1×1) surface. Similarly, when the surface coverage of CO drops below a second critical value, the surface reconstructs back into the hex arrangement. Whereas the CO sticking coefficient is roughly the same on both surface phases (*79*), the O_2 sticking coefficient on the (1×1) surface is reported to be 100-fold greater than on the hex surface (*11*), leading to the potential for higher reaction rates on this surface phase. CO-induced reconstruction and microfacetting of Pt(110) surfaces have similar effects on the O_2 sticking coefficient and reaction rate.

If we assume that the predominant Pt

crystal face in our samples was Pt(100) under reaction conditions, we can then investigate qualitatively what the possible contribution of reconstruction was in our dynamic experiments. During the period where only O_2 was flowing into the reactor, the Pt surface would have been in the hex phase. When CO was admitted to the reactor, the rapid adsorption of CO would have resulted in an increase in CO coverage beyond the initial critical value and reconstruction to the (1 × 1) phase. Upon reconstruction, the rate of oxygen adsorption would have increased two orders of magnitude, creating a maximum in reaction rate and the initial extra CO_2 peak, before the CO coverage increased to inhibitory levels.

The second extra CO_2 peak is more difficult to explain, however, using the surface reconstruction model. When CO was flushed from the reactor, the CO coverage would have decreased, the surface would have reconstructed back to the hex phase, and the oxygen adsorption rate would have decreased by a factor of 100. This change would have contributed to a sudden decrease in reaction rate, rather than causing the extra CO_2 production peak seen in our data. This result suggests that, whereas reconstruction may have occurred in our samples and affected the shape of the second extra CO_2 peaks, reconstruction did not cause the appearance of the second extra CO_2 peaks.

Adsorption Calorimetry Experiments

Adsorption calorimetry experiments were performed to further explore the differences between the chloride and nitrate samples observed in the steady-state and dynamic reaction studies. Figure 9 presents the results of typical adsorption calorimetry experiments over the chloride Pt/Al_2O_3 sample and a blank Al_2O_3 sample. The curves are plots of sample temperature vs time over 4 min immediately prior to, during, and after CO was rapidly admitted to the chamber. The rapid jump in temperature seen over the Pt/Al_2O_3 sample was due to the heat released during adsorption of CO onto Pt. The temperature decay following the initial jump was due to the heat loss through the thermocouple wires and the CO gas to the surroundings. The blank Al_2O_3 sample showed no initial temperature jump, only a slow rise in temperature following exposure to CO. Three superimposed adsorption runs are shown for the chloride sample in Fig. 10. Note the reproducibility

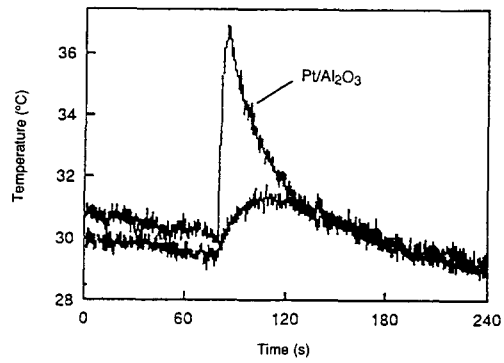

FIG. 9. CO adsorption curves for Pt/Al_2O_3 chloride sample (upper curve) and blank Al_2O_3 sample (lower curve). The temperature of the sample increases rapidly as CO is admitted to the sample chamber and adsorbs, releasing the heat of adsorption. The temperature decays as heat is lost to the surroundings.

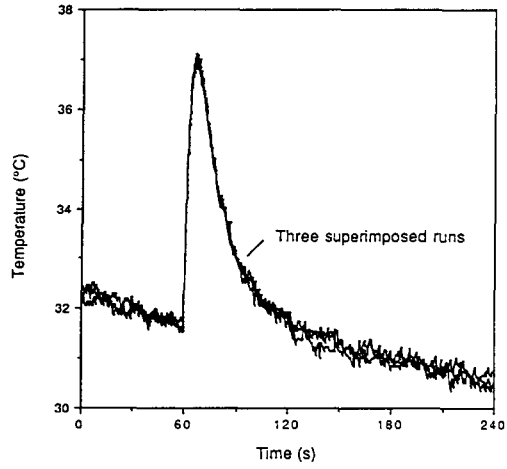

FIG. 10. Three superimposed CO adsorption curves for the chloride sample showing the reproducibility of the adsorption runs.

of the experiments, especially that of the initial temperature jumps.

In this experiment, the system functioned as an isoperibol calorimeter (*99*). An isoperibol calorimeter has a finite heat conductance between the sample and the constant temperature surroundings. Therefore, in this type of calorimeter, the temperature rises as in an adiabatic system, but the temperature decays with time due to the heat loss to the surroundings. The integral heat of adsorption is found by integration of the temperature vs time curve upon dosing of a sample and accounting for the rate of heat loss,

$$\Delta H_{ads} = \frac{1}{N_{co} R_{th}} \int T(t)\, dt$$

where, ΔH_{ads} is the integral heat of adsorption of CO (kcal/mol), N_{co} is moles of CO adsorbed (mol), $T(t)$ is temperature (°C), and R_{th} is the thermal resistance (°C/kcal).

Normally, R_{th} for a system is not determined directly but is determined from the temperature response of a calibration standard. For our experiments, a calibration standard was not available. However, a comparison of the initial temperature jumps over the two samples provides a relative comparison of the integral heats of adsorption. The initial temperature jumps were 4.8 ± 0.2°C/μmol CO adsorbed for the chloride sample and 5.6 ± 0.2°C/μmol CO adsorbed for the nitrate sample. This comparison shows that the integral heat of CO adsorption is 15% greater over the nitrate sample than over the chloride sample. This result supports the conclusion previously drawn from the steady-state and dynamic reaction experiments that the nitrate sample adsorbs CO more strongly than the chloride sample.

Thermal Desorption

Figure 11 shows representative CO desorption spectra for both the chloride and nitrate samples. Desorption of CO during TPD from blank Al_2O_3 support was less than 6% of that desorbed from the Pt/Al_2O_3 samples. The chloride spectrum (Fig. 11a) had four peaks: a shoulder peak on the leading

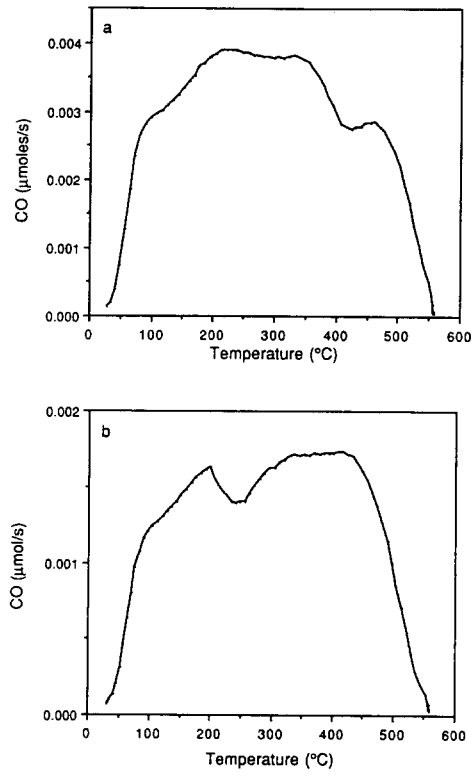

FIG. 11. CO TPD spectra for (a) the chloride sample and (b) the nitrate sample. Temperature ramp rates were 1°C/s.

edge of the spectrum at 85°C, the main peak at 225°C, a secondary peak at 330°C, and a sharp, but smaller, shoulder peak at 460°C on the declining edge of the spectrum. In contrast, the nitrate spectrum (Fig. 11b) showed only three peaks: a shoulder peak at 100°C, a sharp peak at 200°C, and a broad peak containing most of the CO desorption centered around 370°C. A comparison of the location of the main peaks (chloride at 225°C; nitrate at 370°C) suggests that a majority of the Pt adsorption sites in the nitrate sample have higher binding energies for CO than those in the chloride sample.

The signal size for the chloride sample is greater than that of the nitrate sample due to the higher Pt loading in the chloride sample. If the samples had the same CO adsorption characteristics, and if diffusional limita-

tions existed within the samples, then the sample having the higher Pt loading would have shown desorption at higher temperatures. The opposite result was observed. Therefore, if diffusional limitations were contributing to the desorption spectra observed here, they served to lessen the differences between the two samples.

Therefore, the TPD results also show the nitrate sample to adsorb CO more strongly than the chloride sample. This result correlates with the data previously obtained from the dynamic and steady-state reaction results and the adsorption calorimetry experiments. All of the differences observed in these measurements demonstrate that measurement of average Pt dispersion is not sufficient to characterize the activity of a supported Pt catalyst for CO oxidation.

HCl Addition to the Nitrate Sample

An obvious question to ask about the starting compounds chosen for this work is whether chloride from the chloroplatinic acid creates the differences in the adsorption and reaction behaviors between the two samples. To address one aspect of this question, an experiment was designed to determine the possible effect of residual chloride. A solution of hydrochloric acid was prepared to fill the pores of a nitrate sample with chloride to the same Cl-to-Pt ratio that the pores of the chloride sample contained during preparation. A nitrate sample was removed from the sample chamber and the wafer quickly dipped in the solution of HCl. The wafer was then dried in air and placed back into the sample chamber. Adsorption and desorption experiments were then performed on the HCl-treated nitrate sample. The adsorption experiments yielded temperature rises per CO uptake consistent with those of the nitrate sample. A sample TPD spectra from the HCl-treated nitrate sample is shown in Fig. 12.

The spectrum in Fig. 12 is characteristic of the spectrum of the original nitrate sample, containing three main peaks. The shoulder peak shifted to a slightly higher temperature, 110°C, and the second peak broadened and was centered around 250°C. The third peak declined in size, however, it remained centered around 370°C. A fourth peak at 460°C, characteristic of the chloride sample, was not observed. Based on these results, we rule out a large effect of the presence of residual chloride on the CO adsorption properties of the chloride sample. More subtle effects of residual chloride or differences in particle size distribution or particle surface structure between the two samples may be important. Differences in particle size and structure could have been induced by the presence of chloride during the initial impregnation and pretreatment of the chloride sample.

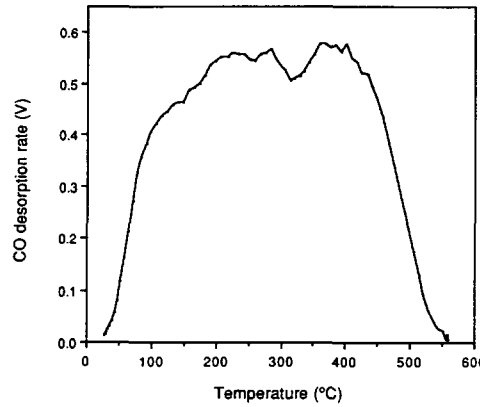

FIG. 12. CO TPD spectra for HCl-treated nitrate sample. Temperature ramp = 1°C/s.

Temperature Effects on Dynamic Response

The effect of temperature on dynamic response has not been previously discussed in this work, but provides some interesting results. Figure 13 shows the effect of temperature on the response times associated with dynamic processes. The CO oxidation cycling experiment performed here consisted of a 23-s cycle, with a 13% duty fraction of CO (3 s on, 20 s off). The O_2 pressure was constant at 330 mTorr, and the CO was cycled between 0 and 120 mTorr. The tem-

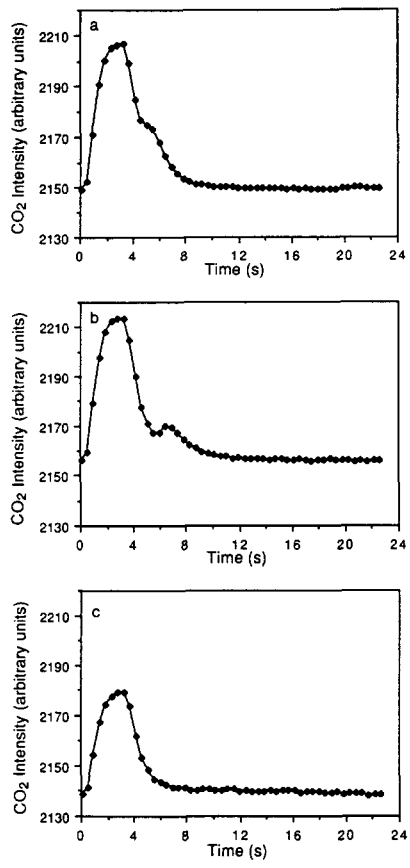

FIG. 13. CO_2 responses for 23-s–13% duty fraction CO cycle between 0 and 120 mTorr at (a) 190, (b) 140, and (c) 90°C. The cycles shown are the averages of 20 successive cycles. The O_2 pressure was constant at 330 mTorr. The tail region for each curve is at the background CO_2 level in the sample chamber.

peratures studied were 90, 140, and 190°C, and the catalyst used for these experiments was the chloride sample.

Figure 13 shows the CO_2 signal (in arbitrary units) for each temperature, averaged over 20 cycles. At 140°C (Fig. 13b), the extra CO_2 peak, seen in Figs. 4 through 6a after switching CO off, was again observed. This extra CO_2 production occurred about 4 s after the CO was switched off, similar to the 24-s–50% duty fraction experiment shown in Fig. 6a. At 190°C (Fig. 13a), the extra CO_2 peak shifted to earlier time onto the shoulder of the initial CO_2 peak. Thus, the response time for extra CO_2 production is faster at higher temperatures. A faster response time for extra CO_2 production is consistent with a faster reaction rate at 190°C. CO coverages obtained during the period where the CO flow is on should also be reduced at higher temperatures.

The 90°C CO_2 response curve in Fig. 13c does not show any obvious extra CO_2 peak. The lower activity level measured compared to the two previous cases is due a slower reaction rate. Although CO coverages obtained during the period where the CO flow is on should be higher at lower temperatures, any extra CO_2 production was probably masked in the tail region due to slow reaction rates at 90°C.

Barshad and Gulari (*14*) examined the effect of temperature on the location of average rate maxima for CO oxidation over Pt/Al_2O_3 in terms of time period–duty fraction space. Their experiments involved periodic alternation of CO and O_2, and the temperatures studied were between 90 and 120°C. As temperature was increased, the optimum cycle period for occurrence of the maximum rate became shorter. Barshad and Gulari proposed that increasing the temperature increased the rate of reaction, thus requiring less time to consume the reactants on the surface following switching of the gas feed. Li *et al.* (*59*) studied the effect of temperature on response times for CO_2 production over Pt/SiO_2 following a step-down in CO and step-up in O_2. Response times were found to decrease significantly as the result of increasing temperature. These previous investigations support our results, which indicate that the response time for reaction of surface adsorbates also decreases with increasing temperature.

Rapid Cycling Responses

One of the principal benefits of the method of instantaneous response analysis is the ability to analyze complex or fast inputs that have no easily predictable outputs. Others have examined the effect of cycling time and duty fraction on reaction rates over

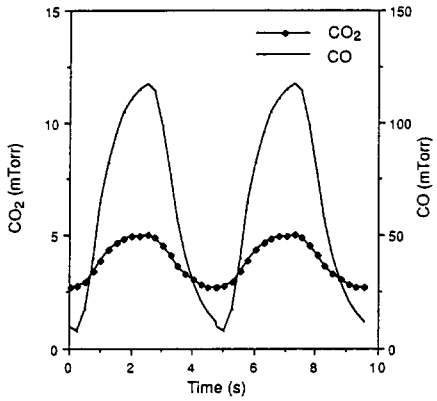

FIG. 14. Rapid cycling CO_2 response to a 5-s–50% duty fraction CO cycle. The figure shows two copies of an identical cycle that is the average of 50 successive cycles. T = 145°C and O_2 pressure = 330 mTorr.

supported noble metals (*13, 14, 16*), however, the time periods studied were usually longer than the response times for peak formation during dynamic cycling experiments. For the dynamic response experiments over the chloride sample presented earlier, the system conditions (330 mTorr O_2, 145°C, and a 24-s–50% duty fraction CO cycle between 0 and 120 mTorr CO) yielded a characteristic response time of approximately 3.5 s for formation of the extra CO_2 peaks after the CO valve was switched on or off. What happens when both the time periods for switching CO are shorter than the characteristic response time for extra CO_2 peak formation?

Figure 14 shows the CO input and the CO_2 response for a rapid cycling experiment under conditions identical to those in Fig. 6 except for the length of cycle. The cycle length was 5 s with a 50% duty fraction, and the catalyst studied was the chloride sample. The graph shows two successive cycles, each averaged over 50 cycles. The CO_2 response appears to be quite simple, with the CO_2 pressure increasing and decreasing in phase with the CO input. However, after applying the instantaneous response method to the data, the catalyst behavior appears more complex. Figure 15 shows both the measured CO_2 response and instantaneous CO_2 response calculated from the steady-state CO oxidation experiments on the chloride sample in Fig. 2a. The differences between the two lines suggest that extra CO_2 was produced as a result of transient surface processes, despite the appearance of the ordinary measured response curve shown in Fig. 14. Figure 16 compares the extra CO_2 produced with the CO input. Since the time period (~2.5 s) when CO was present and absent in the sample chamber were slightly less than the characteristic response time for appearance of extra CO during slow cycling (~3.5 s), the result was extra CO_2 production which occurred out of phase with the CO input. Also, note that the extra CO_2 production has two peaks per cycle: a main peak (seen at 5 s in Fig. 16) and a shoulder peak (seen at 4 s in Fig. 16). The response time for extra CO_2 production (~3.5 s) coupled with the fact that the measured fractional burn-off of adsorbed CO in Fig. 8 was larger than the fractional burn-off of accumulated O atoms during each cycle may account for the location and magnitude of these peaks.

CONCLUSIONS

The considerable differences in behavior between the two Pt/Al_2O_3 samples prepared

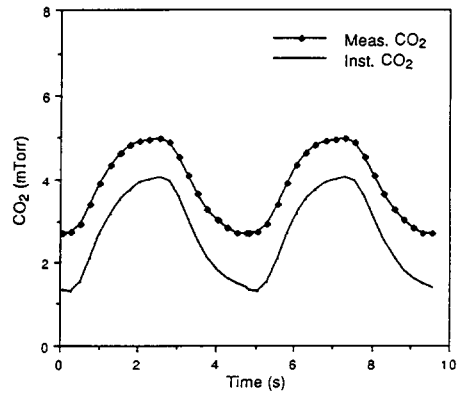

FIG. 15. Measured and instantaneous CO_2 responses for the 5-s–50% duty fraction cycling experiment. T = 145°C and O_2 pressure = 330 mTorr.

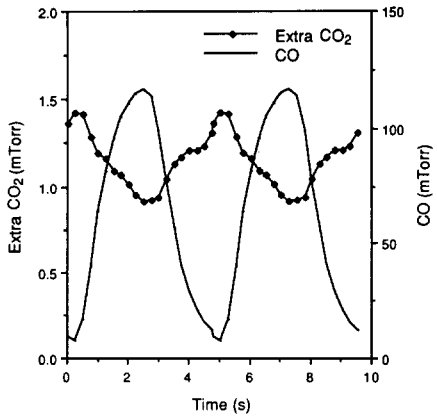

FIG. 16. "Extra" CO_2 produced compared with the CO input for the 5-s–50% duty fraction cycling experiment. T = 145°C and O_2 pressure = 330 mTorr.

from different starting compounds demonstrate that measurement of average Pt dispersion is not sufficient to characterize the performance of a supported Pt catalyst during CO oxidation. Steady-state and dynamic reaction results correlated with each other and with the TPD and adsorption calorimetry results. The results indicate that the sample prepared from tetraamineplatinum nitrate has, on average, stronger CO–Pt interactions than the sample prepared from chloroplatinic acid. Since addition of HCl to the chloride-free catalyst did not have a significant effect on CO adsorption, relatively subtle effects of residual chloride or differences in particle size distribution and particle surface structure, possibly induced by the presence of chloride during sample preparation, may have affected CO adsorption and oxidation behavior. The complex dynamic responses measured over both catalysts demonstrate that transient processes on the catalyst surfaces produced CO_2 at higher rates than would be predicted by instantaneous response to steady-state conditions during dynamic operation. The dynamic experiments on the chloride sample indicate that relatively high CO surface coverages (~25%) may be present under first-order steady-state conditions. Numerical simulations of the experiments are in progress. Preliminary results of the simulations indicate that the combined steady-state and dynamic behavior of the chloride catalyst cannot be predicted by kinetic models specifying random distribution of reactants over a uniform surface of constant activity. This suggests that segregation of adsorbed CO into patches or islands, and/or reconstruction of the Pt surface, may have contributed to the experimental results.

ACKNOWLEDGMENTS

The support of the National Science Foundation through Grants CBT 85-04536 and CBT 87-15427 is gratefully acknowledged.

REFERENCES

1. Wei, J., *Adv. Chem. Ser.* **148,** 1 (1975).
2. Hegedus, L. L., Oh, S. E., and Baron, K., *AIChE J.* **23,** 632 (1977).
3. Golchet, A., and White, J. M., *J. Catal.* **53,** 266 (1978).
4. Haaland, D. M., and Williams, F. L., *J. Catal.* **76,** 450 (1982).
5. Sales, B. C., Turner, J. E., and Maple, M. B., *Surf. Sci.* **103,** 54 (1981).
6. Rathousky, J., and Hlavacek, V., *J. Catal.* **75,** 122 (1982).
7. Böcker, D., and Wicke, E., *in* "Temporal Order" (L. Rensing and N. I. Jaeger, Eds.), p. 75. Springer-Verlag, Berlin, 1984.
8. Lynch, D. T., and Wanke, S. E., *J. Catal.* **88,** 333 (1984).
9. Razon, L. F., Chang, S.-M., and Schmitz, R. A., *Chem. Eng. Sci.* **41,** 1561 (1986).
10. Sant, R., and Wolf, E. E., *J. Catal.* **110,** 249 (1988).
11. Ertl, G., Norton, P. R., and Rusting, J., *Phys. Rev. Lett.* **49,** 177 (1982).
12. Cox, M. P., Ertl, G., and Imbihl, R., *Phys. Rev. Lett.* **54,** 1725 (1985).
13. Cutlip, M. B., *AIChE J.* **25,** 502 (1979).
14. Barshad, Y., and Gulari, E., *AIChE J.* **31,** 649 (1985).
15. Barshad, Y., Zhou, X., and Gulari, E., *J. Catal.* **94,** 128 (1985).
16. Zhou, X., Barshad, Y., and Gulari, E., *Chem. Eng. Sci.* **41,** 1277 (1986).
17. Zhou, X., and Gulari, E., *Langmuir* **2,** 715 (1986).
18. Norton, P. R., Goodale, J. W., and Selkirk, E. B., *Surf. Sci.* **83,** 189 (1979).
19. Steininger, J., Lehwald, S., and Ibach, H., *Surf. Sci.* **123,** 264 (1982).
20. Gland, J. L., and Kollin, E. B., *J. Chem. Phys.* **78,** 963 (1983).

21. Taylor, J. L., and Weinberg, W. H., *Surf. Sci.* **78,** 259 (1978).
22. Herz, R. K., and Marin, S. P., *J. Catal.* **65,** 281 (1980).
23. Harold, M. P., and Garske, M. E., *J. Catal.*, in press.
24. Harold, M. P., and Garske, M. E., *J. Catal.*, in press.
25. Tsai, P. K., Wu, M. G., and Maple, M. B., *J. Catal.*, in press.
26. Engel, T., and Ertl, G., *Adv. Catal.* **28,** 1 (1979).
27. Conrad, H., Ertl, G., and Küppers, J., *Surf. Sci.* **76,** 323 (1978).
28. Shigeishi, R. A., and King, D. A., *Surf. Sci.* **75,** L397 (1978).
29. Stuve, E. M., Madix, R. J., and Brundle, C. R., *Surf. Sci.* **146,** 155 (1984).
30. Behm, R. J., Thiel, P. A., Norton, P. R., and Bindner, P. E., *Surf. Sci.* **147,** 143 (1984).
31. Barteau, M. A., Ko, E. I., and Madix, R. J., *Surf. Sci.* **104,** 161 (1981).
32. Akhter, S., and White, J. M., *Surf. Sci.* **171,** 527 (1986).
33. Norton, P. R., Goodale, J. W., and Creber, D. K., *Surf. Sci.* **119,** 411 (1982).
34. Mundschau, M., Kordesch, M. E., Rausenberger, B., Engel, W., Bradshaw, A. M., and Zeitler, E., *Surf. Sci.* **227,** 246 (1990).
35. Rotermund, H. H., Engel, W., Kordesch, M., and Ertl, G., *Nature* **343,** 355 (1990).
36. McCabe, R. W., and Schmidt, L. D., *Surf. Sci.* **66,** 101 (1977).
37. McClellan, M. R., Gland, J. L., and McFeeley, F. R., *Surf. Sci.* **112,** 63 (1981).
38. Hopster, H., Ibach, H., and Comsa, G., *J. Catal.* **46,** 37 (1977).
39. Hayden, B. E., Kretzschmar, K., Bradshaw, A. M., and Greenler, R. C., *Surf. Sci.* **149,** 394 (1985).
40. Foger, K., *in* "Catalysis Science and Technology" (J. R. Anderson and M. Boudart, Eds.) Vol. 6, p. 227. Springer-Verlag, Berlin, 1984.
41. Vannice, M. A., Hasselbring, L. C., and Sen, B. J., *J. Catal.* **97,** 66 (1986).
42. Herskowitz, M., Holliday, R., Cutlip, M. B., and Kenney, C. N., *J. Catal.* **74,** 408 (1982).
43. Akubuiro, E. C., Verykios, X. E., and Lesnick, L., *Appl. Catal.* **14,** 215 (1985).
44. Flytzani-Stephanopoulos, M., and Schmidt, L. D., *Prog. Surf. Sci.* **9,** 83 (1979).
45. Amariglio, A., and Amariglio, H., *J. Catal.* **68,** 86 (1981).
46. Ladas, S., Imbihl, R., and Ertl, G., *Surf. Sci.* **198,** 42 (1988).
47. Jaeger, N. I., Möller, K., and Plath, P. J., *J. Chem. Soc. Faraday Trans. 1* **82,** 3315 (1986).
48. Ladas, S., Imbihl, R., and Ertl, G., *Surf. Sci.* **219,** 88 (1989).
49. Herz, R. K., and Shinouskis, E. J., *Appl. Surf. Sci.* **19,** 373 (1984).
50. Bennett, C. O., Laporta, L. M., and Cutlip, M. B., *in* "Studies in Surface Science and Catalysis" (A. Crucq, and A. Frennet, Eds.), Vol. 30, p. 143. Elsevier, Amsterdam, 1987.
51. Wei, J., and Becker, E. R., *ACS Adv. Chem. Ser.* **143,** 166 (1975).
52. Cho, B. K., *Ind. Eng. Chem. Fundam.* **22,** 410 (1983).
53. Oh, S. H., Baron, K., Cavendish, J. C., and Hegedus, L. L., *ACS Symp. Ser.* **65,** 461 (1978).
54. Bennett, C. O., *Catal. Rev. Sci. Eng.* **13,** 121 (1976).
55. Kobayashi, M., and Kobayashi, H., *Catal. Rev. Sci. Eng.* **10,** 139 (1974).
56. Yang, C. C., Cutlip, M. B., and Bennett, C. O., *in* "Proceedings, 5th International Congress on Catalysis, Palm Beach, 1972" (J. W. Hightower, Ed.), Vol. 1, p. 273. Elsevier, New York, 1973.
57. Lyberatos, G., Kuszta, B., and Bailey, J. E., *Chem. Eng. Sci.* **39,** 739 (1984).
58. Cutlip, M. B., Yang, C. C., and Bennett, C. O., *AIChE J.* **18,** 1073 (1972).
59. Li, Y.-E., Böcker, D., and Gonzales, R. D., *J. Catal.* **110,** 319 (1988).
60. Dwyer, S. M., and Bennett, C. O., *J. Catal.* **75,** 275 (1982).
61. Vaporciyan, G., Annapragada, A., and Gulari, E., *Chem. Eng. Sci.* **43,** 2957 (1988).
62. Graham, W. R. C., and Lynch, D. T., *in* "Studies in Surface Science and Catalysis" (J. W. Ward, Ed.), Vol. 38, p. 693. Elsevier, Amsterdam, 1988.
63. Cant, N. W., and Donaldson, R. A., *J. Catal.* **71,** 320 (1981).
64. Shigeishi, R. A., and King, D. A., *Surf. Sci.* **75,** L397 (1978).
65. Su, E. C., Rothschild, W. G., and Yao, H. C., *J. Catal.* **118,** 111 (1989).
66. Mukesh, D., Morton, W. Kenney, C. N., and Cutlip, M. B., *Surf. Sci.* **138,** 237 (1984).
67. Goodman, M. G., Cutlip, M. B., Kenney, C. N., Morton, W., and Mukesh, D., *Surf. Sci.* **120,** L453 (1982).
68. Graham, W. R. C., and Lynch, D. T., *Surf. Sci.* **187,** L633 (1987).
69. Dumont, M., Poraiux, M., and Dagonnier, R., *Surf. Sci.* **169,** L307 (1986).
70. Ziff, R. M., Gulari, E., and Garshad, Y., *Phys. Rev. Lett.* **56,** 2553 (1986).
71. Araya, P., Porod, W., and Wolf, E. E., *Surf. Sci.* **230,** 245 (1990).
72. Silverberg, M., Ben-Shaul, A., and Rebentrost, F., *J. Chem. Phys.* **83,** 6501 (1985).
73. Silverberg, M., and Ben-Shaul, A., *J. Chem. Phys.* **87,** 3178 (1987).
74. Fichthorn, K. A., Ziff, R. A., and Gulari, E., *in* "Studies in Surface Science and Catalysis" (J. W.

Ward, Ed.), Vol. 38, p. 883. Elsevier, Amsterdam, 1988.
75. Kaul, D. J., Sant, R., and Wolf, E. E., *Chem. Eng. Sci.* **42,** 1399 (1987).
76. Kaul, D. J., and Wolf, E. E., *J. Catal.* **89,** 348 (1984).
77. Lynch, D. T., *Chem. Eng. Sci.* **39,** 1325 (1984).
78. Thiel, P. A., Behm, R. J., Norton, P. R., and Ertl, G., *Surf. Sci.* **121,** L553 (1982).
79. Behm, R. J., Thiel, P. A., Norton, P. R., and Ertl, G., *J. Chem. Phys.* **78,** 7437 (1983).
80. Ladas, S., Imbihl, R., and Ertl, G., *Surf. Sci.* **197,** 153 (1988).
81. Ladas, S., Imbihl, R., and Ertl, G., *Surf. Sci.* **198,** 42 (1988).
82. Imbihl, R., Sander, M., and Ertl, G., *Surf. Sci.* **204,** L701 (1988).
83. Schwartz, S. B., and Schmidt, L. D., *Surf. Sci.* **183,** L269 (1987).
84. Schüth, F., and Wicke, E., *Ber. Bunsenges. Phys. Chem.* **93,** 191 (1989).
85. Lynch, D. T., Emig, G., and Wanke, S. E., *J. Catal.* **97,** 456 (1986).
86. Ajayan, P. M., and Marks, L. D., *Phys. Rev. Lett.* **63,** 279 (1989).
87. Ajayan, P. M., and Marks, L. D., paper presented at the 199th ACS National Meeting, Boston, April 22–27, 1990.
88. Cho, B. K., and Stock, C. J., *J. Catal.* **117,** 202 (1989).
89. Prairie, M. R., Cho, B. K., Oh, S. H., Shinouskis, E. J., and Bailey, J. E., *Ind. Eng. Chem. Res.* **27,** 1396 (1988).
90. Fogler, H. S., "Elements of Chemical Reaction Engineering," 1st ed., p. 422. Prentice–Hall, Englewood Cliffs, NJ, 1986.
91. Petersen, E. E., "Chemical Reaction Analysis," p. 132. Prentice–Hall, Englewood Cliffs, NJ, 1965.
92. Pt/SiO_2 sample characterized and provided by Dr. M. A. Vannice, Penn State Univ.
93. Herz, R. K., and Sell, J. A., *J. Catal.* **94,** 166 (1985).
94. Herz, R. K., *in* "Studies in Surface Science and Catalysis" (A. Crucq, and A. Frennet, Eds.), Vol. 30, p. 427. Elsevier, Amsterdam, 1987.
95. Pawlicki, P. C., and Schmitz, R. A., *Chem. Eng. Prog.* **83(2),** 40 (1987).
96. Kaul, D. J., and Wolf, E. E., *J. Catal.* **93,** 321 (1985).
97. Lindstrom, T. H., and Tsotsis, T. T., *Surf. Sci.* **167,** L194 (1986).
98. Tsai, P. K., Maple, M. B., and Herz, R. K., *J. Catal.* **113,** 453 (1988).
99. Hemminger, W., and Höhne, G., "Calorimetry—Fundamentals and Practice," Verlag Chemie, Weinheim, 1984.